

1 **Physical processes of cooling and megadrought in 4.2 ka BP event:**
2 **results from TraCE-21ka simulations**

3
4 Mi Yan^{1,2}, Jian Liu^{1,2*}

5 ¹Key Laboratory of Virtual Geographic Environment, Ministry of Education; State
6 key Laboratory of Geographical Environment Evolution, Jiangsu Provincial
7 Cultivation Base; School of Geographical Science, Nanjing Normal University,
8 Nanjing, 210023, China

9 ²Jiangsu Center for Collaborative Innovation in Geographical Information Resource
10 Development and Application, Nanjing, 210023, China

11
12 *jliu@njnu.edu.cn

13
14
15

Abstract

16
17 It is widely believed that multidecadal to centennial cooling and drought occurred from
18 4500 BP to 3900 BP, known as the 4.2 ka BP event that triggered the collapse of several
19 cultures. However, whether this event was a global event or a regional event and what
20 caused this event remain unclear. In this study, we investigated the spatiotemporal
21 characteristics, the possible causes and the related physical processes of the event using
22 a set of long-term climate simulations, including one all-forcing experiment and four
23 single-forcing experiments. The results derived from the all-forcing experiment show
24 that this event occurs over most parts of the Northern Hemisphere (NH), indicating that
25 this event could have been a hemispheric event. The cooler NH and warmer Southern
26 Hemisphere (SH) illustrate that this event could be related to the slowdown of the
27 Atlantic Meridional Overturning Circulation (AMOC). The comparison between the
28 all-forcing experiment and the single-forcing experiments indicates that this event
29 might be caused by internal variability, while external forcings such as orbital and
30 greenhouse gases might have modulation effects. A positive North Atlantic Oscillation
31 (NAO)-like pattern in the atmosphere (low troposphere) triggered a negative Atlantic
32 Multidecadal Oscillation (AMO)-like pattern in the ocean, which then triggered a
33 Circumglobal Teleconnection (CGT)-like wave train pattern in the atmosphere (high
34 troposphere). The positive NAO-like pattern and the CGT-like pattern are the direct
35 physical processes that lead to the NH cooling and megadrought. The AMO-like pattern
36 plays a “bridge” role in maintaining this barotropic structure in the atmosphere at a
37 multidecadal-centennial time scale. Our work provides a global image and dynamic
38 background to help better understand the 4.2 ka BP event.

39

40

41

42 **1 Introduction**

43 Understanding the characteristics and mechanisms of climate changes during the
44 Holocene can help predicting future changes. The multidecadal-to-centennial abrupt
45 climate change, or the rapid climatic change during ca. 4.5-3.9 ka BP (before 1950 CE),
46 the so called “4.2 ka BP event”, was one of the major climate events during the
47 Holocene (Wang, 2009; Staubwasser and Weiss, 2006; Mayewski et al., 2004; Wang,
48 2010). This event is considered to be closely linked to the cultural evolutions of
49 different regions of Eurasia such as the collapse of the Akkadian empire, the termination
50 of the urban Harappan civilization in the Indus valley and the collapse of Neolithic
51 Cultures around the Central Plain of China (Weiss et al., 1993; Weiss and Bradley, 2001;
52 Wu and Liu, 2001; Staubwasser et al., 2003; Wu and Liu, 2004; An et al., 2005;
53 Staubwasser and Weiss, 2006; Liu et al., 2013; Weiss, 2015, 2016). Moreover, this event
54 is also thought to be the transition of the Middle to Late Holocene (Walker et al., 2012;
55 Finkenbinder et al., 2016). However, the characteristics, causes and corresponding
56 mechanisms behind this event remain unclear.

57 The 4.2 ka BP event is mostly characterized by rapid events at various latitudes
58 (Jansen et al., 2007), e.g., cooling in Europe (Lauritzen, 2003), centennial
59 megadroughts in North America (Booth et al., 2005), decreased precipitation in both
60 southern and northern China (Tan et al., 2008), and the weakened summer monsoon in
61 India (Nakamura et al., 2016); however, the manifestation of this event is far from
62 convincing and needs more evidence and simulation investigations (Roland et al., 2014).
63 Many reconstructions have shown that the 4.2 ka BP event is dominated by
64 megadroughts at centennial-scale over mid-low latitudes (Tan et al., 2008; Yang et al.,
65 2015; Weiss, 2016). However, Roland et al. (2014) found no compelling evidence, at
66 least in peatland records, to support that there was a 4.2 ka BP event in Great Britain
67 and Ireland. Moreover, according to the hydrologic cycle (i.e. the hydroclimate changes
68 are often regionally specific), it cannot be ruled out that there were no flooding events
69 somewhere else during this period. For example, Huang et al. (2011) and Tan et al.
70 (2018) found that successive floods occurred over the middle reaches of the Yellow
71 River in China in association with the abrupt climatic event of 4.2 ka BP.

72 Understanding the causes and mechanisms of the 4.2 ka BP event can provide
73 explanations for the reconstructed discrepancies over different regions. For the causes
74 of the event, some reconstruction and modeling studies have suggested that the solar
75 irradiance could have played an important role in the early Holocene climate changes
76 (Wang et al., 2005; Rupper et al., 2009; Owen and Dortch, 2014); however, no strong
77 evidence has shown that the solar irradiance affected glacier fluctuations (cooling
78 events) in the late Holocene since there is yet no good mechanistic explanations of how
79 small changes in solar irradiance could significantly affect large scale climate changes
80 (Solomina et al., 2015). Tan et al. (2008) thought that the 4.2 ka BP event could have
81 been induced by the southward shift of the Intertropical Convergence Zone (ITCZ) and
82 oceanic sea surface temperature (SST) changes, as well as the vegetation feedback
83 caused by the solar activity. Liu et al. (2013) and Deininger et al. (2017) argued that the
84 atmospheric circulation, such as the North Atlantic Oscillation (NAO)-like pattern but
85 on a centennial time scale, could have played a more important role than the ocean
86 circulation in this event, although the mechanisms that forced the circulation change
87 remained unclear. A new reconstruction study has also shown that the dry phases over
88 the western Mediterranean in the period of 4.5 ka BP-2.8 ka BP generally agreed with
89 positive NAO conditions (Ramos-Román et al., 2018). However, studies come to
90 different conclusions on the likely phase of the NAO-like patter during the late
91 Holocene (Finkenbinder et al., 2016). Some studies show positive NAO-type patterns
92 during the late Holocene (Tremblay et al., 1997; Sachs, 2007; Ramos-Román et al.,
93 2018), whereas others show negative NAO-like patterns (Rimbu et al., 2004). Since the
94 mechanisms could be a complex set of air-sea interactions (Roland et al., 2014), it is
95 hard for reconstruction to provide a general record due to its limitations such as
96 interpretation and spatially incompleteness. The mechanisms behind the 4.2 ka BP
97 event need to be clarified.

98 Therefore, to improve understanding of the 4.2 ka BP event, new high-resolution
99 reconstruction studies that focus on the 4.2 ka BP event are required. On the other hand,
100 physical-based modeling research can provide general concepts of the characteristics
101 of the event along with the causes and the mechanisms. Climate simulations have been

102 conducted to investigate another abrupt cooling event in the early Holocene, the so-
103 called 8.2 ka BP event. The simulations were used to test the hypothesis raised by the
104 reconstruction studies that the 8.2 ka BP event was most likely caused by freshwater
105 forcing and was associated with weakening of the Atlantic Meridional Overturning
106 Circulation (AMOC) (Morrill et al., 2013; Wagner et al., 2013; Morrill et al., 2014;
107 Matero et al., 2017; Ljung et al., 2008; Alley and Agustsdottir, 2005). For example, the
108 simulations argued that the meltwater from the collapse of the ice dome over Hudson
109 Bay was an essential forcing of the 8.2 ka BP event (Wagner et al., 2013; Matero et al.,
110 2017). However, little modeling work has been applied to the 4.2 ka BP event.

111 Recently, Ning et al. (2019) briefly compared the spatial patterns of climate change
112 in the 9th and 5th millennia BP using a set of transient modeling results on a long-term
113 perspective. In the present study, we will use the same set of simulation results to
114 provide an in-depth characteristics of the 4.2 ka BP event and will focus on the possible
115 causes and mechanisms behind this event. The model and experiments are introduced
116 in Sect. 2. The results are shown in Sect. 3. The possible causes and mechanisms are
117 discussed in Sect. 4, and conclusions are drawn in Sect. 5.

118

119 **2 Model and experiments**

120 A set of transient simulations (TraCE-21ka, Simulation of Transient Climate
121 Evolution over the past 21,000 years, He, 2011) conducted with the Community
122 Climate System model version 3 (CCSM3) was used to investigate the spatial and
123 temporal characteristics of the 4.2 ka BP event and to determine the possible causes and
124 mechanisms behind this event. The experiments are listed in Table 1, including one
125 transient experiment with all-forcings (TraCE-ALL), one single-forcing experiment
126 forced only by transient orbital variation (TraCE-ORB), one single-forcing experiment
127 forced only by transient melt-water flux (TraCE-MWF), one single-forcing experiment
128 forced only by quasi-transient ice-sheet (TraCE-ICE), and one single-forcing
129 experiment forced only by transient greenhouse gases concentrations changes (TraCE-
130 GHG). The simulations were conducted from 22000 BP to 1990 CE for the TraCE-ALL,
131 the TraCE-ORB and the TraCE-GHG experiments, and from 19000 BP to 1990 CE for

132 the TraCE-MWF and the TraCE-ICE experiments.

133 The transient June insolation changes at 60°N and 60°S that resulted from the
134 orbital variation and the transient CO₂ change used in the simulations are shown in Fig.
135 1. The continental ice-sheet and topography changes are based on the ICE-5G (VM2)
136 reconstruction (He et al., 2013; Peltier, 2004). For the geography changes, the Barents
137 Sea opens at 13.1 ka BP, the Bering Strait opens at 12.9 ka BP, Hudson Bay opens at
138 7.6 ka BP, and the Indonesian Throughflow opens at 6.2 ka BP. The freshwater injected
139 into Northern Hemisphere (NH) and Southern Hemisphere (SH) oceans are based on
140 specific time slices (e.g., 19 ka BP into North Atlantic, 17 ka BP into North Atlantic,
141 11.5 ka BP into Arctic, St. Lawrence River, Hudson Strait, Barents Sea, North Sea, Ross
142 Sea and Weddell Sea). Note that no freshwater was delivered to the ocean after 5000
143 BP in the TraCE-ALL and TraCE-MWF experiments. The detailed information about
144 the experiments design can be referred to He (2011) and He et al. (2013).

145 The TraCE-21ka simulation was evaluated with reconstructions and was found
146 that it could reproduce major deglacial temperature evolutions (Clark et al., 2012;
147 Shakun et al., 2012). It has been used to depict the causes and mechanisms of Holocene
148 climate changes, such as the Bølling-Allerød warming (Liu et al., 2009), cooling into
149 the Younger Dryas and recovery to warm conditions (Liu et al., 2012) and the ENSO
150 evolution over the past 21 ka (Liu et al., 2014a). In the present work, we adopted the
151 period of 5000 BP-3000 BP to focus on the 4.2 ka BP event.

152

153 **3 Results**

154 3.1 Identification of 4.2 ka BP event in the model simulation

155 The 101-year running mean annual NH surface temperature and precipitation
156 during 5 ka BP-3 ka BP shows double peak centennial cooling and drought from 4.4 ka
157 BP to 4.0 ka BP (Fig. 2, dashed black line). However, the variabilities are smaller over
158 the SH than those over the NH. There is no significant cooling and drought event during
159 that period (Fig. S1, dashed black line) over the SH. The SH precipitation even shows
160 a double-peak wet condition during the period of 4.4 ka BP-4.0 ka BP.

161 The double peak centennial cooling and drought are still obvious when the 31-year

162 running mean is applied to the time series (not shown), which indicates that the
163 simulated climate events potentially comparable to the 4.2 ka event. Moreover, the
164 centennial warming periods right before and after the cooling event indicate that this
165 event might be included in a quasi-millennium variation. Therefore, the 4.2 ka BP event
166 could be a multiscale event, i.e. from multi-decadal to millennium.

167 The seasonal mean NH surface temperature changes show that the annual mean
168 variability is dominated by the boreal winter (December-January-February, DJF)
169 surface temperature change (Fig. S2). The correlation coefficient between the annual
170 mean NH surface temperature (NHT) and the DJF mean NHT is 0.96 (after the 101-
171 year running mean), which is significant above the 99% confidence level, much higher
172 than the correlation coefficient between the annual mean and the boreal summer (June-
173 July-August, JJA) mean of only 0.30 (after the 101-year running mean), which is not
174 significant. However, this is different for the precipitation change, for which both the
175 JJA mean and the DJF mean contribute to the annual mean precipitation change (not
176 shown).

177 To identify the characteristics of the 4.2 ka BP event, two centennial cool periods
178 and two centennial warm periods that exceeded ± 0.5 standard deviations are selected.
179 The two centennial cool periods span from 4320 BP to 4220 BP and from 4150 BP to
180 4050 BP, and the two centennial warm periods span from 4710 BP to 4610 BP and from
181 3980 BP to 3880 BP.

182

183 3.2 Spatial characteristics of surface temperature and precipitation

184 To help draw a coherent global view of the 4.2 ka BP event, the spatial
185 characteristics of temperature and precipitation changes during the 4.2 ka BP event are
186 shown in Fig. 3.

187 Figure 3a gives the spatial distribution of the annual mean surface temperature
188 difference between the cold periods and the warm periods. The cooling significantly
189 occurred over most regions of the NH, especially over the middle to high latitudes of
190 the NH and most land regions of the SH. Most parts of India, northern Mexico and the
191 middle latitudes of the SH ocean experienced warm conditions. Such asymmetric

192 change between the hemispheres (cool NH and warm SH) favors the southward shift of
193 the ITCZ. The spatial distribution of the surface temperature change is still dominated
194 by the boreal winter pattern (not shown). The large cooling over the NH and small
195 warming over the SH could be related to the orbital change (Fig. S3), which induces
196 insolation increasing over the SH but decreasing over the NH.

197 The spatial distribution of annual mean precipitation differences between the cold
198 periods and the warm periods is shown in Fig. 3b. During the cold periods, significant
199 drought is mainly located over many land regions of the NH, especially over Europe,
200 western Asia, and interior North America and Central America. The significant dry
201 conditions over the Dead Sea, the Gulf of Omen, interior North America and western
202 North Africa and the wet condition over South America are consistent with the
203 reconstructions (Yechieli et al., 1993; Cullen et al., 2000; Forman et al., 1995; Marchant
204 and Hooghiemstra, 2004). For the SH, the land precipitation increased, which indicates a
205 southward shift of the ITCZ, as suggested by the aforementioned asymmetric
206 temperature change and by the previous studies based on both reconstructions
207 (Fleitmann et al., 2007; Cai et al., 2012) and simulations (Broccoli et al., 2006). Over
208 East China, the precipitation anomalies show a wet south-dry north pattern, which
209 indicates a weakened East Asian monsoon revealed by the reconstruction record (Tan
210 et al., 2018). However, the simulated anomaly pattern is not very significant over East
211 China. This might be related to the model resolution, the model performance, or the
212 actual climate change. Therefore, simulations with higher resolution, inter-model and
213 model-data comparisons are required to draw a clearer view about the climate change
214 over East China.

215 The sea surface temperature (SST) shows that the largest change occurs over the
216 northern Atlantic Ocean and then the northern Pacific Ocean (Fig. 4). The warmer south
217 and cooler north over the Atlantic Ocean indicates an Atlantic Multi-Decadal
218 Oscillation (AMO)-like pattern with its cold phase. The cold phase of the AMO has
219 been confirmed to induce summer rainfall decreases over India and Sahel in both
220 simulations and proxy data (Zhang and Delworth, 2006; Shanahan et al., 2009).

221 The simulated characteristics of the temperature change, the precipitation change,

222 and the SST change are similar to those responses to the weakened AMOC state
223 (Vellinga and Wood, 2002; Zhang and Delworth, 2005; Delworth and Zeng, 2012;
224 Brown and Galbraith, 2016) (Fig. S4).

225

226 3.3 Circulations associate with the 4.2 ka BP event

227 The sea level pressure (SLP) differences between the cooler periods and the
228 warmer periods show that the largest change occurs over the mid-high latitudes of the
229 NH and SH (Fig. 5a). The negative SLP anomalies over the high North Atlantic and
230 positive SLP anomalies over the middle North Atlantic during the cool periods resemble
231 a positive North Atlantic Oscillation (NAO)-like pattern but on a centennial-millennial
232 time scale. The positive NAO-like pattern is accompanied by cyclonic circulation over
233 Iceland and anticyclonic circulation over the Azores Islands and thus strengthened
234 westerlies over the downstream regions (Fig. 5a). The subtropical highs and the relative
235 anticyclones in both the SH and NH are strengthened during the cold periods from low
236 troposphere (850 hPa) to high troposphere (200 hPa), which illustrates a barotropic
237 structure (Fig. 5). Note that the strengthened subtropical highs over the NH are most
238 significant at low level (sea level and 850 hPa), while the subtropical highs over the SH
239 are most significant at high level (200 hPa). The centers with positive geopotential
240 height anomalies during the 4.2 ka BP event over Western Europe, Central Asia, East
241 Asia, the east north Pacific and Eastern North America, as well as the anti-cyclonic
242 circulation anomalies at 200 hPa (Fig. 5d), resemble a Circumglobal Teleconnection
243 (CGT)-like wave pattern (Ding and Wang, 2005; Lin et al., 2016) but on a centennial-
244 millennial time scale.

245 The strengthened subtropical highs with mid-latitudes anticyclones from lower to
246 upper levels are the direct physical processes that cause the precipitation decreases and
247 thus the following megadrought over mid-latitudes of NH regions, particularly over
248 Eurasia. The cooler land-warmer ocean over East Asia and the West Pacific (Fig. 3a)
249 indicate weakened land-ocean thermal contrast associated with significantly higher SLP
250 over land and lower SLP over the adjacent ocean (insignificant) (Fig. 5a). The
251 weakened land-ocean contrast can lead to a weaker East Asian monsoon, accompanied

252 by precipitation increases over the southern China pattern and precipitation decreases
253 over the northern China pattern (Fig. 3b). Such conclusion is very rough, since the
254 simulated anomaly patterns are not very significant. More investigations with higher
255 resolutions of modeling and reconstruction works are required to get satisfactory results.

256

257 **4 Discussions**

258 The simulations show that the cool and dry conditions of the 4.2 ka BP event is
259 more like a hemispheric phenomenon, mainly located over the NH, rather than a global
260 phenomenon. The land over the SH experiences cool but wet conditions, and the mid-
261 latitude SH ocean is warmer. The potential causes and mechanisms of this event will be
262 discussed in this section.

263 4.1 The possible causes of the 4.2 ka BP event

264 Some records suggested that solar irradiance was one of the essential mechanisms
265 that drove the Holocene climate variation at centennial to millennial time scales (Bond
266 et al., 2001), whereas others suggested that the linkage between solar irradiance and
267 multicentury scale cooling events during the Holocene was weak, particularly in the
268 mid- to late-Holocene (Turney et al., 2005; Wanner et al., 2008). Changes in solar
269 irradiance are not included in the experiments used in the present work. Nonetheless,
270 we still obtain multicentury cooling events (such as the 4.2 ka BP event) in the TraCE-
271 ALL experiment, but with smaller magnitude. This side-fact indicates that the solar
272 irradiance might not be the driving factor for the Holocene cooling events.

273 If the results derived from the TraCE-ALL experiment are consistent with those
274 derived from a particular single-forcing sensitivity experiment, we assume the variation
275 to be forced by that forcing. Otherwise, if the results derived from the TraCE-ALL
276 experiment differ from those from the single-forcing sensitivity experiments, we
277 assume the variation to be forced by the internal variability. In this section, we use the
278 series after applications of 101-year running means as an example and compare the
279 results derived from the all-forcing experiment to those derived from the single-forcing
280 experiment to determine the possible forcings that triggered the 4.2 ka BP event.

281 The correlation coefficients between the annual mean NHT derived from the

282 TraCE-ALL run and the NHT derived from each single-forcing run are listed in Table
283 2. A two-sided Students t-test is used for the statistical significant test, assuming 20
284 degrees of freedom, which is estimated simply from a 2000-year time series subjected
285 to a 100-year running mean (Delworth and Zeng, 2012). There is no significant clue
286 that the annual mean NHT variation is forced by the orbital variation or the other
287 forcings due to the non-significant correlations. During the period of 5000 BP - 3000
288 BP, the variation of simulated JJA mean NHT is likely forced by the solar radiation due
289 to the orbital variation (Table 2; the correlation coefficient between the two series is
290 0.79 at $p<0.05$), whereas the greenhouse gas change has a comparable negative impact
291 on the JJA mean NHT (the correlation coefficient is -0.73 at $p<0.05$). The melt-water
292 flux also has a moderate contribution to the JJA mean NHT change (the correlation
293 coefficient is 0.48 at $p<0.05$). For the DJF mean NHT, only melt-water flux has a
294 notable negative effect (the correlation coefficient is -0.43 at $p<0.05$). However, there
295 is no meltwater forcing during this period, so the NHT change can be taken as internal
296 variability. Therefore, the significant correlation coefficient between the all forcing run
297 result and the meltwater forcing run result might be a coincidence, due to the
298 autocorrelation of internal variability. This is another side-fact indicating the cold
299 events during the late Holocene might be related to the internal variability. Note that if
300 the effective degree of freedom is used, none of the abovementioned correlation
301 coefficients are significant. The effective degree of freedom is calculated by the
302 following equation:

$$303 \quad N_{dof} = N \times \frac{1 - r_1 \times r_2}{1 + r_1 \times r_2}$$

304 where N_{dof} is the effective degree of freedom regarding to the two correlation samples,
305 N is the total sample size, r_1 and r_2 are autocorrelation lag-1 values for sample 1 and
306 sample 2, respectively (Bretherton et al., 1999).

307 On the other hand, the annual mean NHT difference between the TraCE-ALL run
308 and the sum of the 4 single-forcing sensitivity experiments shows variation similar to
309 the NHT derived from the TraCE-ALL run from 5000 BP to 3000 BP (Fig. S5). The
310 correlation coefficient between these two time-series is 0.66, which is significant above

311 the 95% confidence level (assuming 20 degrees of freedom). We assume the difference
312 between the TraCE-ALL run and the sum of the 4 single forcing runs to be the internal
313 variation, taking that the climate responses to the external forcings are linear at global
314 and hemispheric scales. Therefore, the internal variation might play a dominant role in
315 the climatic variation during the period of 5000 BP-3000 BP. However, the linearity of
316 the climate responding to the external forcings need further clarification, since there
317 would be interactions between each forcing and between forcings and internal
318 variability.

319 Moreover, there is no double-peak cooling event during the period of 4400 BP-
320 4000 BP in any single forcing run (Fig. 1, colored lines), which indicates that the 4.2
321 ka BP event might not be triggered by those external forcings, including the orbital, the
322 melt-water flux, the ice-sheets and the greenhouse gases in isolation. Volcanic eruptions
323 have been identified as one of the important drivers of climate variation, whereas there
324 were few eruptions during 4400 BP-4000 BP (Sigl et al., 2018). Therefore, we conclude
325 that the variability relating to the 4.2 ka BP event might be driven by the internal
326 variability. Klus et al. (2017) also suggested that the internal climate variability could
327 trigger abrupt cold events in the North Atlantic without external forcings (e.g., solar
328 irradiance or volcanic).

329 However, why such large variation due to the internal variability occurs at
330 approximately 4.2 ka BP remains unknown. There is little ice-sheet change and no melt
331 water discharge after 5.0 ka BP in the TraCE-ICE run and TraCE-MWF run, and the
332 variations of climate derived from these two runs can thus be considered as internal
333 variabilities. The multicentennial cooling events can also be found in the standardized
334 NHT during the last 5000 years of the two experiments (Fig. S6), and there are drought
335 events in the standardized NH precipitation time series (not shown). However, the
336 timing of those cooling and drought events occurs stochastically. This indicates a
337 general concept of the random variation of the internal mode of the climate system.
338 There is a reduction of NH temperature and precipitation at around 4600 BP in the
339 TraCE-ORB (Fig. 2, orange lines), which might be related to the timing of the event as
340 speculated by Ning et al. (2019).

341 Ning et al. (2019) compared the 5th millennium BP cooling with the 9th millennium
342 cooling and concluded that the 9th millennium BP cooling was resulted from the
343 freshwater forcing while the orbital forcing is the most likely explanation of cooling in
344 the North Atlantic starting from the early 5th Millennium BP through most of the later
345 Holocene, but with fluctuations. In the present work, we attribute this fluctuation to the
346 internal variability, which is superposed on the orbital induced long-term trend. This
347 work and Ning et al.'s work (2019) focus on different aspects and different time scales,
348 and are complementary to better understand the 4.2 ka BP event.

349

350 4.2 The mechanisms of the centennial-millennial cooling and drought

351 As has mentioned in Sec. 3.3, the low level NAO-like pattern and upper level
352 CGT-like pattern are the direct mechanisms that cause cooling and megadroughts over
353 most part of the NH. Previous studies also proposed that the temperature and
354 precipitation changes over Eurasia and Africa were directly linked to the NAO (Cullen
355 et al., 2002; Kushnir and Stein, 2010). The first leading mode of the Empirical
356 Orthogonal Function (EOF) of the annual mean SLP during 5 ka BP-3 ka BP shows a
357 double-peak positive NAO-like pattern but on a centennial scale during the period of
358 4400 BP-4000 BP (Fig. 6). The first leading EOF of geopotential height at 200 hPa after
359 application of a 31-year running mean shows a CGT-like pattern and similar double-
360 peak variation during the period of 4400 BP-4000 BP, which is more obvious after
361 applying the 101-year running mean (Fig. 7). This means that the double-peak cooling
362 and drought of the 4.2 ka BP event could be strongly related to the double peak positive
363 NAO-like pattern (at low level) and CGT-like pattern (at high level) at a centennial time
364 scale.

365 Li et al. (2013) suggested that the NAO is a predictor of NHT multidecadal
366 variability during the 20th century. In this study, significant correlation is also found
367 between the annual mean NAO index and the annual mean NHT during the period of
368 4400 BP-4000 BP, with the NAO leading by approximately 40 years (Fig. 8). The NAO
369 index is defined by the first leading mode of the EOF of the SLP. The regressed annual
370 mean surface temperature against the NAO index 40 years earlier during 4400 BP and

371 4000 BP shows cooler NH high latitudes and a warmer SH (Fig. S7), especially the
372 cooling over the northern North Atlantic Ocean, Europe, East Asia and North America.

373 The geopotential height at 200 hPa regressed against the SST over the two North
374 Atlantic outstanding regions (Fig. 4) shows a CGT-like pattern after application of a
375 31-year running mean (Fig. 9), which is similar to the conclusion from Lin et al. (2016)
376 that the CGT could be excited by the AMO-related SST anomaly. The regressed 200
377 hPa geopotential height shows a similar pattern after application of a 101-year running
378 mean (not shown). The anticyclones associated with CGT-like pattern over the West
379 Europe, Central Asia and North America can suppress the precipitation and thus lead to
380 megadrought over these regions.

381 Considering the NAO-like pattern, the CGT-like pattern and the AMO-like pattern
382 together, we suggest that the AMO could be playing a “bridge” role to keep the
383 barotropic structure at the centennial scale, which is similar to the synthesis proposed
384 by Li et al. (2013) that the AMO is a “bridge” that links the NAO and NHT at a
385 multidecadal timescale. Delworth and Zeng (2016) suggested that the NAO variation
386 had significant impact on the AMOC and the subsequent influence on the atmosphere
387 and large-scale climate at multidecadal-centennial time scales. Other studies also
388 focused on the role of SST anomalies over the North Pacific and North Atlantic oceans
389 when investigating the possible mechanisms of the 4.2 ka BP event (Kim et al., 2004;
390 Marchant and Hooghiemstra, 2004; Booth et al., 2005).

391 We notice the centennial-millennial variation of the AMOC after the mid-
392 Holocene in the all forcing run (Fig. S4a). There also exists a double peak variation
393 during the period of 4400-4000, accompanied by the similar spatial patterns of
394 temperature and precipitation anomalies as the simulated 4.2 ka BP event (Fig. S4b, c).
395 However, whether this AMOC variation is related to the external forcing, such as the
396 orbital forcing, or just the internal variability remains unknown, and needs further
397 investigations.

398

399 **5 Conclusion**

400 The characteristics of the 4.2 ka BP event along with the potential drivers and the

401 mechanisms are investigated using a set of transient climate simulations. The simulated
402 event is characterized by hemispheric cooling and megadrought over the NH, whereas
403 the SH experiences warming (over mid-latitude ocean) and wet conditions during this
404 event. The annual mean temperature change is dominated by the boreal winter change.
405 The cool and dry NH and warm and wet SH pattern indicates a southward shift of the
406 ITCZ, as suggested by the reconstructions. These characteristics could also be related
407 to a weakening of the AMOC, which needs further investigation.

408 By comparison between the all-forcing experiment and the single-forcing
409 sensitivity experiments, the 4.2 ka BP event can largely be attributed to the internal
410 variability, although the orbital forcing and the greenhouse gases could impact the
411 boreal summer NHT variation. The origin could be in polar regions and the North
412 Atlantic and may influence the NH climate through teleconnections such as the NAO-
413 like pattern and the CGT-like pattern. The positive NAO-like pattern in the atmosphere
414 triggers cooling over the NH and the negative AMO-like pattern in the ocean, which
415 may last for decades or even centuries. The negative AMO-like pattern triggers CGT-
416 like wave patterns at a multidecadal-centennial time scale accompanied by anticyclones
417 over West Europe, Central Asia and North America, which induce megadrought over
418 those regions. The simplified diagram of the mechanism is shown in Fig. 10.

419 Our findings provide a global pattern and mechanical background of the 4.2 ka BP
420 event that can help better understanding this event. We attribute the internal variabilities
421 to be an essential forcing of the 4.2 ka BP event. However, whether or not the external
422 forcings have modulation effects need to be clarified. For example, is the timing of the
423 event stochastic due to the internal variability or modulated by the external forcings
424 such as the orbital changes? Why the SST forcing in the North Atlantic can be
425 maintained at a multidecadal-centennial time scale requires more study. Current results
426 are mainly based on annual mean precipitation and temperature, whereas the impacts
427 of external forcings may have seasonal dependence; further investigations are required
428 to evaluate these impacts.

429 The model responses to the external forcings are small, especially in the Holocene
430 because of the absence of a significant change of the AMOC and the meltwater forcing

431 after 6 ka (Liu et al., 2014b). So we use the amplified anomalies between the cold and
432 warm periods, rather than simply the cold anomalies against the long-term average, to
433 illustrate the mechanisms of the event. We need to keep in mind that we still might not
434 be modeling the events comparable to the 4.2 ka BP event, particularly during the late
435 Holocene. More model-data, inter-model and inter-events comparisons are required to
436 better understand the cold events during the Holocene.

437

438

439 **Acknowledgments**

440 We acknowledge Prof. Bin Wang and two anonymous referees for the
441 comments helping to clarify and improve the paper. This research was jointly
442 supported by the National Key Research and Development Program of China (grant
443 no. 2016YFA0600401), the National Basic Research Program (grant no.
444 2015CB953804), the National Natural Science Foundation of China (grant nos.
445 41671197, 41420104002 and 41631175), Open Funds of State Key Laboratory of
446 Loess and Quaternary Geology, Institute of Earth Environment, CAS
447 (SKLLQG1820), and the Priority Academic Development Program of Jiangsu Higher
448 Education Institutions (PAPD, grant no. 164320H116). TraCE-21ka was made
449 possible by the DOE INCITE computing program, and supported by NCAR, the
450 NSFP2C2 program, and the DOE Abrupt Change and EaSM programs.
451

452 **References:**

- 453 Alley, R., and Agustsdottir, A.: The 8k event: cause and consequences of a major Holocene abrupt
454 climate change, *Quaternary Science Reviews*, 24, 1123-1149, 10.1016/j.quascirev.2004.12.004,
455 2005.
- 456 An, C.-B., Tang, L., Barton, L., and Chen, F.-H.: Climate change and cultural response around 4000
457 cal yr B.P. in the western part of Chinese Loess Plateau, *Quaternary Research*, 63, 347-352,
458 10.1016/j.yqres.2005.02.004, 2005.
- 459 Bond, G., Kromer, B., Beer, J., Muscheler, R., Evans, M. N., Showers, W., Hoffmann, S., Lotti-
460 Bond, R., Hajdas, I., and Bonani, G.: Persistent solar influence on North Atlantic climate during
461 the Holocene, *Science*, 294, 2130, 2001.
- 462 Booth, R. K., Jackson, S. T., Forman, S. L., Kutzbach, J. E., Bettis, I. E. A., Kreig, J., and Wright,
463 D. K.: A severe centennial-scale drought in mid-continental North America 4200 years ago and
464 apparent global linkages, *The Holocene*, 15, 321-328, 2005.
- 465 Bretherton, C. S., Widmann, M., Dymnikov, V. P., Wallace, J. M., and Bladé, I.: The effective
466 number of spatial degrees of freedom of a time-varying field, *J. Climate*, 12(7), 1990-2009,
467 1999.
- 468 Broccoli, A. J., Dahl, K. A., and Stouffer, R. J.: Response of the ITCZ to Northern Hemisphere
469 cooling, *Geophysical Research Letters*, 33, L01702, 10.1029/2005gl024546, 2006.
- 470 Brown, N., and Galbraith, E. D.: Hosed vs. unhosed: interruptions of the Atlantic Meridional
471 Overturning Circulation in a global coupled model, with and without freshwater forcing,
472 *Climate of the Past*, 12, 1663-1679, 10.5194/cp-12-1663-2016, 2016.
- 473 Cai, Y., Zhang, H., Cheng, H., An, Z., Lawrence Edwards, R., Wang, X., Tan, L., Liang, F., Wang,
474 J., and Kelly, M.: The Holocene Indian monsoon variability over the southern Tibetan Plateau
475 and its teleconnections, *Earth and Planetary Science Letters*, 335-336, 135-144,
476 10.1016/j.epsl.2012.04.035, 2012.
- 477 Clark, P. U., Shakun, J. D., Baker, P. A., Bartlein, P. J., Brewer, S., Brook, E., Carlson, A. E., Cheng,
478 H., Kaufman, D. S., Liu, Z., Marchitto, T. M., Mix, A. C., Morrill, C., Otto-Bliesner, B. L.,
479 Pahnke, K., Russell, J. M., Whitlock, C., Adkins, J. F., Blois, J. L., Clark, J., Colman, S. M.,
480 Curry, W. B., Flower, B. P., He, F., Johnson, T. C., Lynch-Stieglitz, J., Markgraf, V., McManus,
481 J., Mitrovica, J. X., Moreno, P. I., and Williams, J. W.: Global climate evolution during the last
482 deglaciation, *Proceedings of the National Academy of Sciences of the United States of America*,
483 109, E1134-1142, 10.1073/pnas.1116619109, 2012.
- 484 Cullen, H. M., Kaplan, A., Arkin, P. A., and DeMenocal, P. B.: Impact of the North Atlantic
485 Oscillation on Middle Eastern climate and streamflow, *Climatic Change*, 55, 315-338, 2002.
- 486 Cullen, H., deMenocal, P., Hemming, S., Hemming, G., Brown, F. H., Guilderson, T., and Sirocko,
487 F.: Climate change and the collapse of the Akkadian empire: Evidence from the deep sea,
488 *Geology*, 28, 379-382, 2000.
- 489 Deininger, M., McDermott, F., Mudelsee, M., Werner, M., Frank, N., and Mangini, A.: Coherency
490 of late Holocene European speleothem $\delta^{18}O$ records linked to North Atlantic Ocean circulation,
491 *Climate Dynamics*, 49, 595-618, 10.1007/s00382-016-3360-8, 2017.
- 492 Delworth, T. L., and Zeng, F.: Multicentennial variability of the Atlantic meridional overturning
493 circulation and its climatic influence in a 4000 year simulation of the GFDL CM2.1 climate
494 model, *Geophysical Research Letters*, 39, L13702, 10.1029/2012gl052107, 2012.
- 495 Delworth, T. L., and Zeng, F.: The Impact of the North Atlantic Oscillation on Climate through Its

496 Influence on the Atlantic Meridional Overturning Circulation, *Journal of Climate*, 29, 941-962,
497 10.1175/jcli-d-15-0396.1, 2016.

498 Ding, Q., and Wang, B.: Circumglobal Teleconnection in the Northern Hemisphere summer, *Journal*
499 *of Climate*, 18, 3483-3505, 2005.

500 Finkenbinder, M. S., Abbott, M. B., and Steinman, B. A.: Holocene climate change in
501 Newfoundland reconstructed using oxygen isotope analysis of lake sediment cores, *Global and*
502 *Planetary Change*, 143, 251-261, 10.1016/j.gloplacha.2016.06.014, 2016.

503 Fisher, D., Osterberg, E., Dyke, A., Dahl-Jensen, D., Demuth, M., Zdanowicz, C., Bourgeois, J.,
504 Koerner, R. M., Mayewski, P., Wake, C., Kreutz, K., Steig, E., Zheng, J., Yalcin, K., Goto-
505 Azuma, K., Luckman, B., and Rupper, S.: The Mt Logan Holocene—late Wisconsinan isotope
506 record: tropical Pacific—Yukon connections, *The Holocene*, 18, 667-677,
507 10.1177/0959683608092236, 2008.

508 Fleitmann, D., Burns, S. J., Mangini, A., Mudelsee, M., Kramers, J., Villa, I., Neff, U., Al-Subbary,
509 A. A., Buettner, A., Hippler, D., and Matter, A.: Holocene ITCZ and Indian monsoon dynamics
510 recorded in stalagmites from Oman and Yemen (Socotra), *Quaternary Science Reviews*, 26,
511 170-188, 10.1016/j.quascirev.2006.04.012, 2007.

512 Forman, S., Oglesby, R., Markgraf, V., and Stafford, T.: Paleoclimatic significance of Late
513 Quaternary eolian deposition on the Piedmont and High Plains, Central United States, *Global*
514 *and Planetary Change*, 11, 35-55, 1995.

515 He, F., Shakun, J. D., Clark, P. U., Carlson, A. E., Liu, Z., Otto-Bliesner, B. L., and Kutzbach, J. E.:
516 Northern Hemisphere forcing of Southern Hemisphere climate during the last deglaciation,
517 *Nature*, 494, 81-85, 10.1038/nature11822, 2013.

518 He, F.: Simulating Transient Climate Evolution of the Last deglaciation with CCSM3, Doctor of
519 Philosophy, Atmospheric and Oceanic Sciences, University of Wisconsin-Madison, 161 pp.,
520 2011.

521 Huang, C. C., Pang, J., Zha, X., Su, H., and Jia, Y.: Extraordinary floods related to the climatic event
522 at 4200 a BP on the Qishuihe River, middle reaches of the Yellow River, China, *Quaternary*
523 *Science Reviews*, 30, 460-468, 10.1016/j.quascirev.2010.12.007, 2011.

524 Jansen, E., Overpeck, J. T., Briffa, K. R., Duplessy, J.-C., Joos, F., Masson-Delmotte, V., Olago, D.,
525 Otto-Bliesner, B., Peltier, W. R., Rahmstorf, S., Ramesh, R., Raynaud, D., Rind, D. H.,
526 Solomina, O., Villalba, R., and Zhang, D.: Palaeoclimate. In: *Climate Change 2007: The*
527 *Physical Science Basis*. , Cambridge University Press, Cambridge, United Kingdom and New
528 York, NY, USA, 2007.

529 Kim, J.-H., Rimbu, N., Lorenz, S. J., Lohmann, G., Nam, S.-I., Schouten, S., Rühlemann, C., and
530 Schneider, R. R.: North Pacific and North Atlantic sea-surface temperature variability during
531 the Holocene, *Quaternary Science Reviews*, 23, 2141-2154, 10.1016/j.quascirev.2004.08.010,
532 2004.

533 Klus, A., Prange, M., Varma, V., Tremblay, L. B., and Schulz, M.: Abrupt cold events in the North
534 Atlantic in a transient Holocene simulation, *Climate of the Past Discussions*, 1-23, 10.5194/cp-
535 2017-106, 2017.

536 Kushnir, Y., and Stein, M.: North Atlantic influence on 19th–20th century rainfall in the Dead Sea
537 watershed, teleconnections with the Sahel, and implication for Holocene climate fluctuations,
538 *Quaternary Science Reviews*, 29, 3843-3860, 10.1016/j.quascirev.2010.09.004, 2010.

539 Lauritzen, S.-E.: Reconstruction of Holocene climate records from speleothems, in: *Global Change*

540 in the Holocene, edited by: Mackay, A., Battarbee, R., Birks, H. J. B., and Oldfield, F., Arnold,
541 London, 242-263, 2003.

542 Li, J., Sun, C., and Jin, F.-F.: NAO implicated as a predictor of Northern Hemisphere mean
543 temperature multidecadal variability, *Geophysical Research Letters*, 40, 5497-5502,
544 10.1002/2013gl057877, 2013.

545 Lin, J.-S., Wu, B., and Zhou, T.-J.: Is the interdecadal circumglobal teleconnection pattern excited
546 by the Atlantic multidecadal Oscillation?, *Atmospheric and Oceanic Science Letters*, 9, 451-
547 457, 10.1080/16742834.2016.1233800, 2016.

548 Liu, J. Q., Lv, H. Y., Negendank, J. F. W., Mingram, J., Luo, X. J., Wang, W. Y., and Chu, G. Q:
549 Cyclic of the Holocene climate variability in Huguangyan Maar lake, China, *Chinese Science*
550 *Bulletin (in Chinese)*, 45, 1190-1195, 2000.

551 Liu, Y. H., Sun, X., and Guo, C. Q.: Records of 4.2 ka BP Holocene Event from China and Its Impact
552 on Ancient Civilizations, *Geological Science and Technology Information (in Chinese)*, 32, 99-
553 106, 2013.

554 Liu, Z. Y., Otto-Bliesner, B., He, F., Brady, E. C., Tomas, R. A., Clark, P. U., Carlson, A. E., Lynch-
555 Stieglitz, J., Curry, W., Brook, E., Erickson, D. J., Jacob, R., Kutzbach, J., and Cheng, J.:
556 Transient simulation of Last Deglaciation with a new mechanism for Bolling-Allerod Warming,
557 *Science*, 325, 310-314, 2009.

558 Liu, Z., Carlson, A. E., He, F., Brady, E. C., Otto-Bliesner, B. L., Briegleb, B. P., Wehrenberg, M.,
559 Clark, P. U., Wu, S., Cheng, J., Zhang, J., Noone, D., and Zhu, J.: Younger Dryas cooling and
560 the Greenland climate response to CO₂, *Proceedings of the National Academy of Sciences of*
561 *the United States of America*, 109, 11101-11104, 10.1073/pnas.1202183109, 2012.

562 Liu, Z., Lu, Z., Wen, X., Otto-Bliesner, B. L., Timmermann, A., and Cobb, K. M.: Evolution and
563 forcing mechanisms of El Niño over the past 21,000 years, *Nature*, 515, 550-553,
564 10.1038/nature13963, 2014a.

565 Liu, Z., Zhu, J., Rosenthal, Y., Zhang, X., Otto-Bliesner, B. L., Timmermann, A., Smith, R. S.,
566 Lohmann, G., Zheng, W., and Elison Timm, O.: The Holocene temperature conundrum,
567 *Proceedings of the National Academy of Sciences of the United States of America*, 111, E3501-
568 3505, 10.1073/pnas.1407229111, 2014b.

569 Ljung, K., Björck, S., Renssen, H., and Hammarlund, D.: South Atlantic island record reveals a
570 South Atlantic response to the 8.2 kyr event, *Clim. Past*, 4, 35-45, 2008.

571 Ma, Z. X., Huang, J. H., Wei, Y., Li, J. H., and Hu, C. Y.: Organic carbon isotope records of the
572 Poyang Lake sediments and their implications for the paleoclimate during the last 8 ka,
573 *Geochimica (in Chinese)*, 33, 279-285, 10.19700/j.0379-1726.2004.03.007, 2004.

574 Marchant, R., and Hooghiemstra, H.: Rapid environmental change in African and South American
575 tropics around 4000 years before present: a review, *Earth-Science Reviews*, 66, 217-260,
576 10.1016/j.earscirev.2004.01.003, 2004.

577 Matero, I. S. O., Gregoire, L. J., Ivanovic, R. F., Tindall, J. C., and Haywood, A. M.: The 8.2 ka
578 cooling event caused by Laurentide ice saddle collapse, *Earth and Planetary Science Letters*,
579 473, 205-214, 10.1016/j.epsl.2017.06.011, 2017.

580 Mayewski, P. A., Rohling, E. E., Curt Stager, J., Karlén, W., Maasch, K. A., Meeker, L. D., Meyerson,
581 E. A., Gasse, F., van Kreveld, S., Holmgren, K., Lee-Thorp, J., Rosqvist, G., Rack, F.,
582 Staubwasser, M., Schneider, R. R., and Steig, E. J.: Holocene Climate Variability, *Quaternary*
583 *Research*, 62, 243-255, 10.1016/j.yqres.2004.07.001, 2004.

584 Morrill, C., LeGrande, A. N., Renssen, H., Bakker, P., and Otto-Bliesner, B. L.: Model sensitivity
585 to North Atlantic freshwater forcing at 8.2 ka, *Climate of the Past*, 9, 955-968, 10.5194/cp-9-
586 955-2013, 2013.

587 Morrill, C., Ward, E. M., Wagner, A. J., Otto-Bliesner, B. L., and Rosenbloom, N.: Large sensitivity
588 to freshwater forcing location in 8.2 ka simulations, *Paleoceanography*, 29, 930-945,
589 10.1002/2014pa002669, 2014.

590 Nakamura, A., Yokoyama, Y., Maemoku, H., Yagi, H., Okamura, M., Matsuoka, H., Miyake, N.,
591 Osada, T., Adhikari, D. P., Dangol, V., Ikehara, M., Miyairi, Y., and Matsuzaki, H.: Weak
592 monsoon event at 4.2 ka recorded in sediment from Lake Rara, Himalayas, *Quaternary*
593 *International*, 397, 349-359, 10.1016/j.quaint.2015.05.053, 2016.

594 Ning, L., Liu, J., Bradley, R. S., and Yan, M.: Comparing the spatial patterns of climate change in
595 the 9th and 5th millennia BP from TRACE-21 model simulations, *Climate of the Past*, 15, 41-
596 52, 10.5194/cp-15-41-2019, 2019.

597 Owen, L. A., and Dortch, J. M.: Nature and timing of Quaternary glaciation in the Himalayan–
598 Tibetan orogen, *Quaternary Science Reviews*, 88, 14-54, 10.1016/j.quascirev.2013.11.016,
599 2014.

600 Peltier, W. R.: GLOBAL GLACIAL ISOSTASY AND THE SURFACE OF THE ICE-AGE EARTH:
601 The ICE-5G (VM2) Model and GRACE, *Annual Review of Earth and Planetary Sciences*, 32,
602 111-149, 10.1146/annurev.earth.32.082503.144359, 2004.

603 Peng, Y., Xiao, J., Nakamura, T., Liu, B., and Inouchi, Y.: Holocene East Asian monsoonal
604 precipitation pattern revealed by grain-size distribution of core sediments of Daihai Lake in
605 Inner Mongolia of north-central China, *Earth and Planetary Science Letters*, 233, 467-479,
606 10.1016/j.epsl.2005.02.022, 2005.

607 Ramos-Román, M. J., Jiménez-Moreno, G., Camuera, J., García-Alix, A., Anderson, R. S., Jiménez-
608 Espejo, F. J., and Carrión, J. S.: Holocene climate aridification trend and human impact
609 interrupted by millennial- and centennial-scale climate fluctuations from a new sedimentary
610 record from Padul (Sierra Nevada, southern Iberian Peninsula), *Climate of the Past*, 14, 117-
611 137, 10.5194/cp-14-117-2018, 2018.

612 Rimbu, N., Lohmann, G., Lorenz, S. J., Kim, J. H., and Schneider, R. R.: Holocene climate
613 variability as derived from alkenone sea surface temperature and coupled ocean-atmosphere
614 model experiments, *Climate Dynamics*, 23, 215-227, 10.1007/s00382-004-0435-8, 2004.

615 Roland, T. P., Caseldine, C. J., Charman, D. J., Turney, C. S. M., and Amesbury, M. J.: Was there a
616 ‘4.2 ka event’ in Great Britain and Ireland? Evidence from the peatland record, *Quaternary*
617 *Science Reviews*, 83, 11-27, 10.1016/j.quascirev.2013.10.024, 2014.

618 Rupper, S., Roe, G., and Gillespie, A.: Spatial patterns of Holocene glacier advance and retreat in
619 Central Asia, *Quaternary Research*, 72, 337-346, 10.1016/j.yqres.2009.03.007, 2009.

620 Sachs, J. P.: Cooling of Northwest Atlantic slope waters during the Holocene, *Geophysical Research*
621 *Letters*, 34, L03609, 10.1029/2006gl028495, 2007.

622 Shakun, J. D., Clark, P. U., He, F., Marcott, S. A., Mix, A. C., Liu, Z., Otto-Bliesner, B., Schmittner,
623 A., and Bard, E.: Global warming preceded by increasing carbon dioxide concentrations during
624 the last deglaciation, *Nature*, 484, 49-54, 10.1038/nature10915, 2012.

625 Shanahan, T. M., Overpeck, J. T., Anchukaitis, K. J., Beck, J. W., Cole, J. E., Dettman, D. L., Peck,
626 J. A., Scholz, C. A., and King, J. W.: Atlantic forcing of persistent drought in West Africa,
627 *Science*, 324, 377-380, 2009.

628 Sigl, M., Severi, M., and McConnell, J. R.: A role for volcanoes in causing the "4.2 ka BP event"?,
629 The 4.2 ka BP event: an international workshop, Pisa, Italy, 2018.

630 Solomina, O. N., Bradley, R. S., Hodgson, D. A., Ivy-Ochs, S., Jomelli, V., Mackintosh, A. N., Nesje,
631 A., Owen, L. A., Wanner, H., Wiles, G. C., and Young, N. E.: Holocene glacier fluctuations,
632 Quaternary Science Reviews, 111, 9-34, 10.1016/j.quascirev.2014.11.018, 2015.

633 Staubwasser, M., and Weiss, H.: Holocene Climate and Cultural Evolution in Late Prehistoric–Early
634 Historic West Asia, Quaternary Research, 66, 372-387, 10.1016/j.yqres.2006.09.001, 2006.

635 Staubwasser, M., Sirocko, F., Grootes, P. M., and Segl, M.: Climate change at the 4.2 ka BP
636 termination of the Indus valley civilization and Holocene south Asian monsoon variability,
637 Geophysical Research Letters, 30, No. 8, 1425, 10.1029/2002gl016822, 2003.

638 Tan, L. C., An, Z. S., Cai, Y. J., and Long, H.: The Hydrological Exhibition of 4.2 ka BP Event in
639 China and Its Global Linkages, Geological Review (in Chinese), 54, 94-104,
640 10.16509/j.georeview.2008.01.010, 2008.

641 Tan, L. C., Cai, Y. J., Cheng, H., Edwards, L. R., Gao, Y. L., Xu, H., Zhang, H. W., and An, Z. S.:
642 Centennial- to decadal- scale monsoon precipitation variations in the upper Hanjiang River
643 region, China over the past 6650 years, Earth and Planetary Science Letters, 482, 580-590,
644 10.1016/j.epsl.2017.11.044, 2018.

645 Thompson, L. G., Mosley-Thompson, E., Davis, M., Henderson, K. A., Brecher, H., Zagorodnov,
646 V. S., Mashiotta, T., Lin, P. N., Mikhaleenko, V. N., Hardy, D. R., and Beer, J.: Kilimanjara Ice
647 Core Records: Evidence of Holocene Climate Change in Tropical Africa, Science, 298, 589-
648 593, 10.1126/science.1073198, 2002.

649 Tremblay, L. B., Mysak, L. A., and Dyke, A. S.: Evidence from driftwood records for century-to-
650 millennial scale variations of the high latitude atmospheric circulation during the Holocene,
651 Geophysical Research Letters, 24, 2027-2030, 10.1029/97gl02028, 1997.

652 Turney, C., Baillie, M., Clemens, S., Brown, D., Palmer, J., Pilcher, J., Reimer, P., and Leuschner,
653 H. H.: Testing solar forcing of pervasive Holocene climate cycles, Journal of Quaternary
654 Science, 20, 511-518, 10.1002/jqs.927, 2005.

655 Vellinga, M., and Wood, R. A.: Global climatic impacts of a collapse of the Atlantic Thermohaline
656 Circulation, Climatic Change, 54, 251-267, 2002.

657 Wagner, A. J., Morrill, C., Otto-Bliesner, B. L., Rosenbloom, N., and Watkins, K. R.: Model support
658 for forcing of the 8.2 ka event by meltwater from the Hudson Bay ice dome, Climate Dynamics,
659 41, 2855-2873, 10.1007/s00382-013-1706-z, 2013.

660 Walker, M. J. C., Berkelhammer, M., Björck, S., Cwynar, L. C., Fisher, D. A., Long, A. J., Lowe, J.
661 J., Newnham, R. M., Rasmussen, S. O., and Weiss, H.: Formal subdivision of the Holocene
662 Series/Epoch: a Discussion Paper by a Working Group of INTIMATE (Integration of ice-core,
663 marine and terrestrial records) and the Subcommission on Quaternary Stratigraphy
664 (International Commission on Stratigraphy), Journal of Quaternary Science, 27, 649-659,
665 10.1002/jqs.2565, 2012.

666 Wang, S. W.: 4.2ka BP Event, Advances in Climate Change Research (in Chinese), 6, 75-76, 2010.

667 Wang, S. W.: Holocene cold events in the North Atlantic: Chronology and Climate Impact,
668 Quaternary Sciences (in Chinese), 29, 1146-1153, 2009.

669 Wang, Y. J., Cheng, H., Edwards, L. R., He, Y. Q., Kong, X. G., An, Z. S., Wu, J. Y., Kelly, M.,
670 Dykoski, C. A., and Li, X. D.: The Holocene Asian Monsoon: Links to Solar Changes and
671 North Atlantic Climate, Science, 308, 854-857, 2005.

672 Wanner, H., Beer, J., Bütikofer, J., Crowley, T. J., Cubasch, U., Flückiger, J., Goosse, H., Grosjean,
673 M., Joos, F., Kaplan, J. O., Küttel, M., Müller, S. A., Prentice, I. C., Solomina, O., Stocker, T.
674 F., Tarasov, P., Wagner, M., and Widmann, M.: Mid- to Late Holocene climate change: an
675 overview, *Quaternary Science Reviews*, 27, 1791-1828, 10.1016/j.quascirev.2008.06.013,
676 2008.

677 Weiss, H., and Bradley, R. S.: What drives societal collapse?, *Science*, 291, 609-610, 2001.

678 Weiss, H., Courty, M. A., Wetterstrom, W., Guichard, F., Senior, L., Meadow, R., and Curnow, A.:
679 The Genesis and Collapse of Third Millennium North Mesopotamian Civilization, *Science*,
680 261, 995-1004, 10.1126/science.261.5124.995, 1993.

681 Weiss, H.: Global megadrought, societal collapse and resilience at 4.2-3.9 ka BP across the
682 Mediterranean and west Asia, *Past Global Change Magazine*, 24, 62-63,
683 10.22498/pages.24.2.62, 2016.

684 Weiss, H.: Megadrought, Collapse, and Resilience in late 3rd millennium BC Mesopotamia, 7th
685 Archaeological Conference of Central Germany, Halle (Saale), 2015.

686 Wu, W. X., and Liu T. S.: 4000aB.P. Event and its implications for the origin of Ancient Chinese
687 Civilization, *Quaternary Sciences (in Chinese)*, 21, 443-451, 2001.

688 Wu, W. X., and Liu, T. S.: Possible role of the “Holocene Event 3” on the collapse of Neolithic
689 Cultures around the Central Plain of China, *Quaternary International*, 117, 153-166,
690 10.1016/s1040-6182(03)00125-3, 2004.

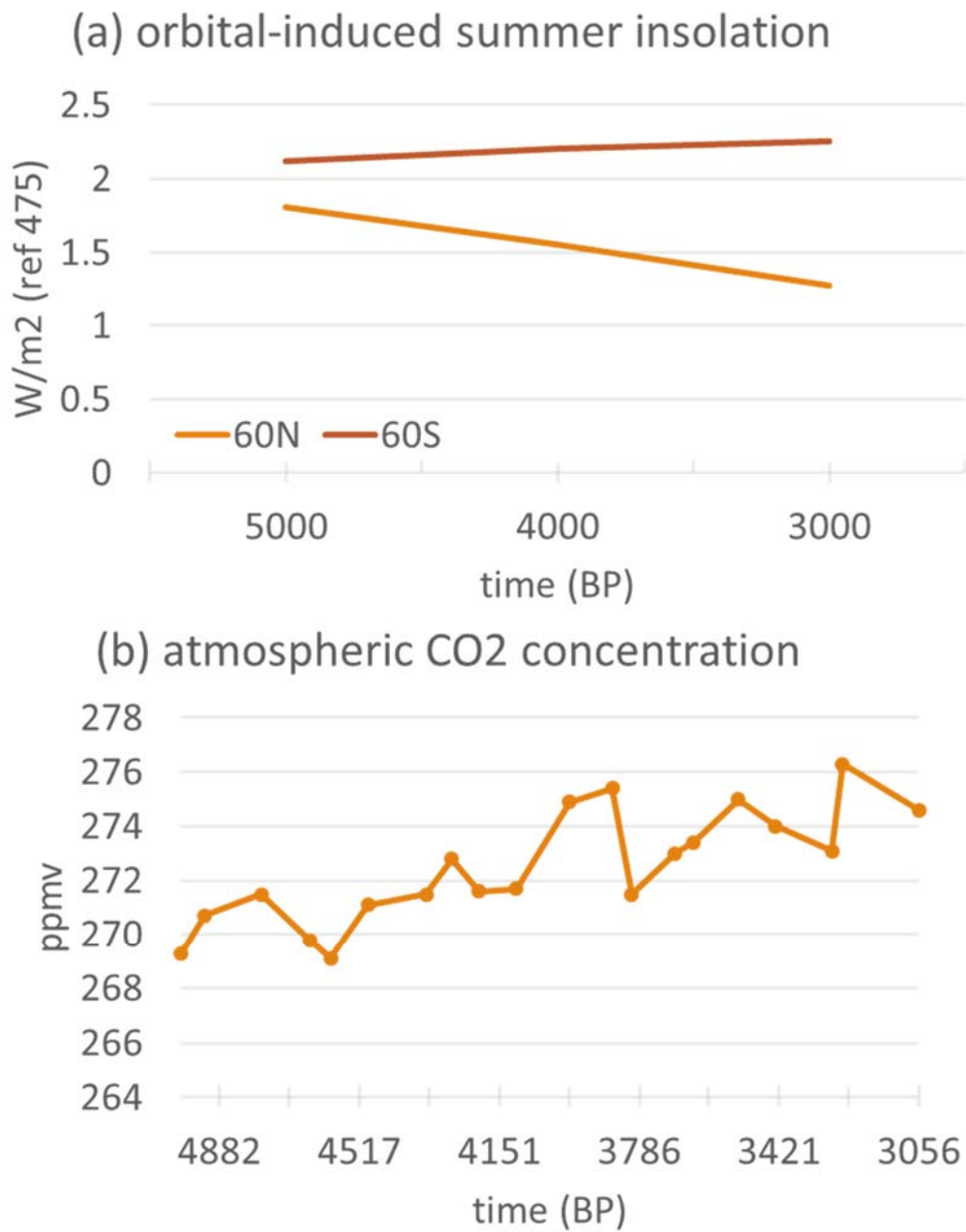
691 Yang, X. P., Scuder, L. A., Wang, X. L., Scuder, L. J., Zhang, D. G., Li, H. W., and al, e.:
692 Groundwater sapping as the cause of irreversible desertification of Hunshandake Sandy Lands,
693 Inner Mongolia, northern China, *PNAS*, 112, 702-706, 2015.

694 Yechieli, Y., Magaritz, M., Levy, Y., Weber, U., Kafri, U., Woelfli, W., and Bonani, G.: Late
695 Quaternary Geological History of the Dead Sea Area, Israel, *Quaternary Research*, 39, 59-67,
696 10.1006/qres.1993.1007, 1993.

697 Zhang, R., and Delworth, T. L.: Simulated Tropical Response to a Substantial Weakening of the
698 Atlantic Thermohaline Circulation, *Journal of Climate*, 18, 1853-1860, 2005.

699 Zhang, R., and Delworth, T. L.: Impact of Atlantic multidecadal oscillations on India/Sahel rainfall
700 and Atlantic hurricanes, *Geophysical Research Letters*, 33, L17712, 10.1029/2006gl026267,
701 2006.

702



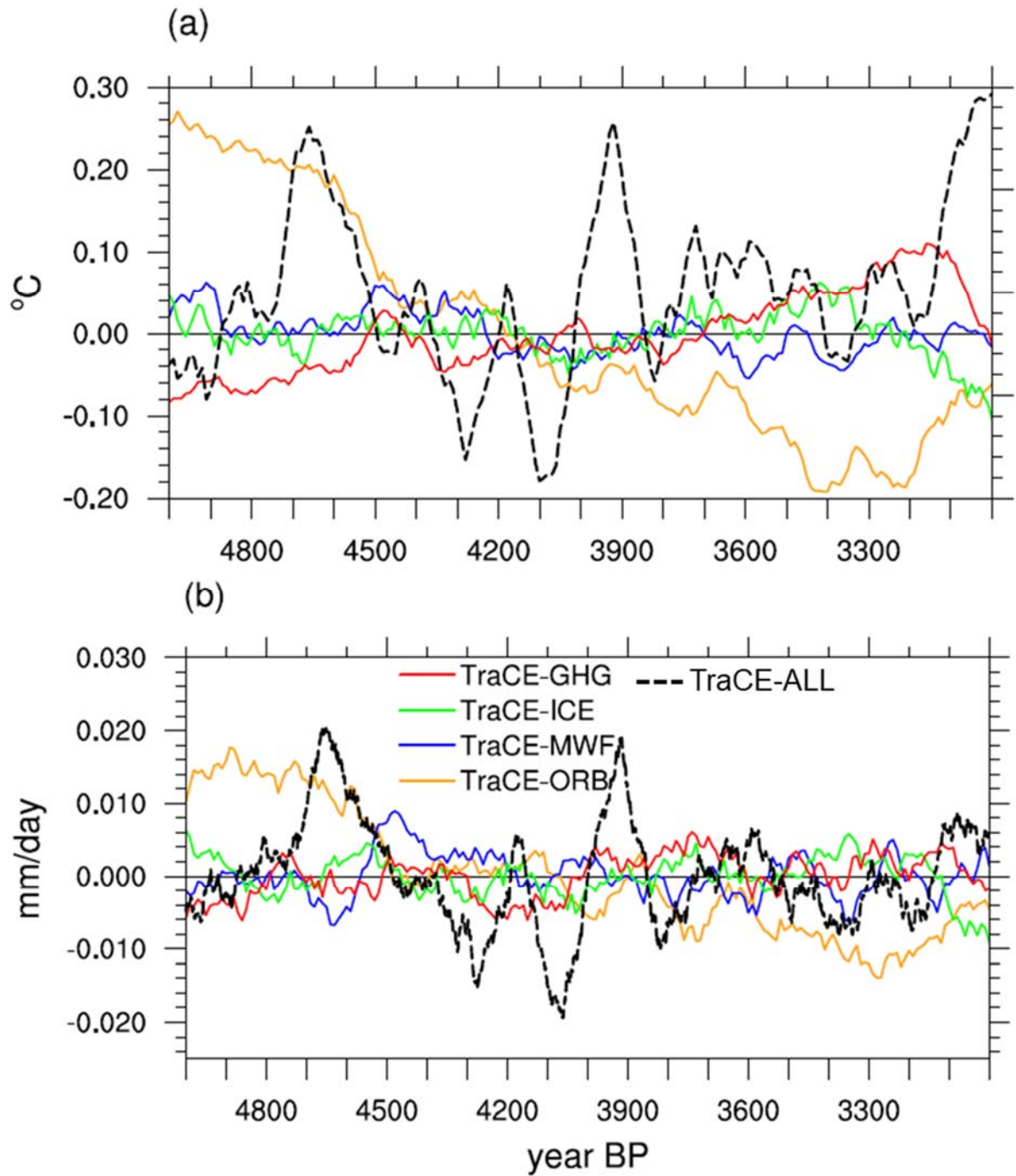
704

705 **Figure 1** Time series of (a) transient summer insolation (at 60°N and 60°S) changes706 resulted from the orbital variation and (b) the transient CO₂ change used in the

707 simulations.

708

709



711

712 **Figure 2** Time series of annual mean NH (a) surface temperature anomalies and (b)

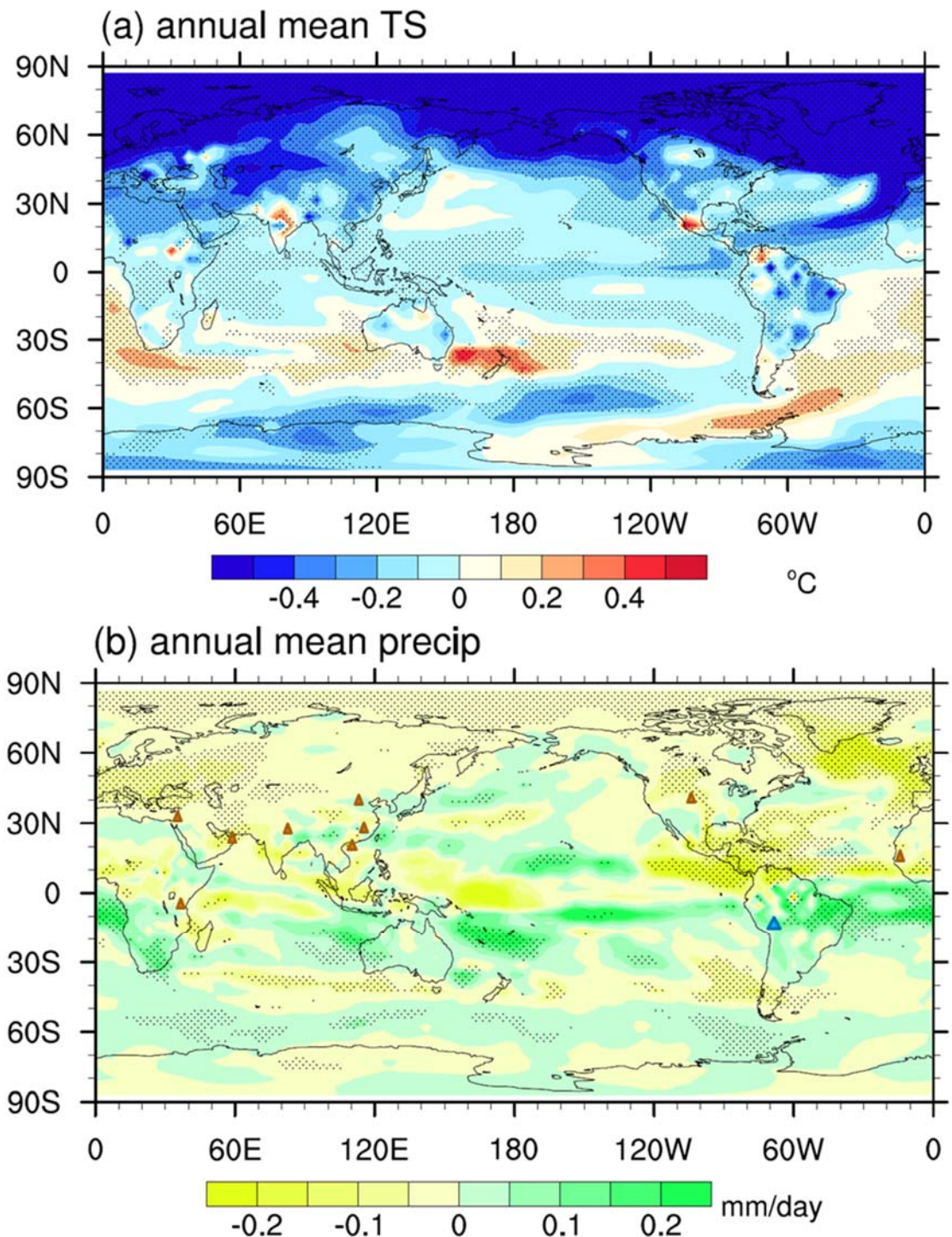
713 precipitation anomalies derived from the TraCE-ALL run (dashed black lines) and

714 each single forcing runs (solid color lines) from 5 ka BP to 3 ka BP. A 101-year

715 running mean has been applied to the time series.

716

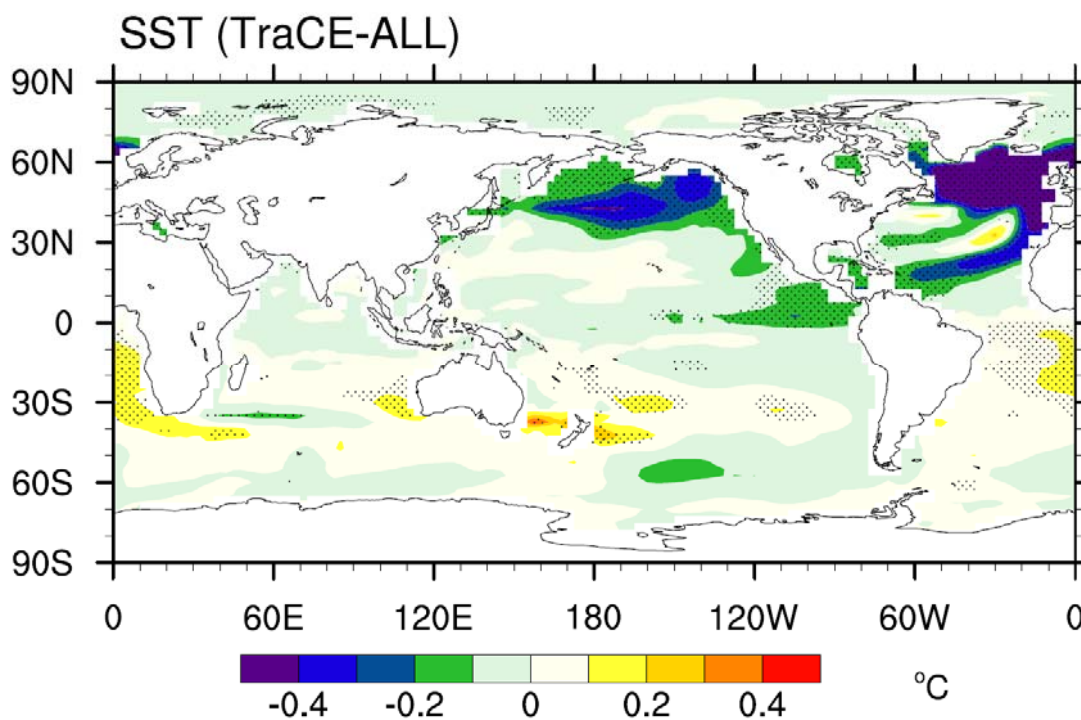
717
718
719



720
721 **Figure 3** Spatial distribution of the annual mean (a) surface temperature and (b)
722 precipitation differences between the cold periods and warm periods derived from the
723 TraCE-ALL run. Those regions where significant above 95% confidence level are
724 dotted. Triangles in (b) denote the dry (orange) and wet (blue) conditions documented

725 in the records, including the following sites: Kilimanjaro (3°04.6'S, 37°21.2'E)
726 (Thompson et al., 2002), Dead Sea (Yechieli et al., 1993), Gulf of Omen (24°23.4'N,
727 59°2.5'E) (Cullen et al., 2000), Lake Rara (29°32'N, 82°05'E) (Nakamura et al.,
728 2016), Maar lake in Huguangyan (21.15°N, 110.29°E) (Liu et al., 2000), Daihai Lake
729 (40.58°N, 112.7°E) (Peng et al., 2005), Poyang Lake (29.15°N, 116.27°E) (Ma et al.,
730 2004), Eastern Colorado Dunes (40°20'N, 104°16'E) (Forman et al., 1995), Lake
731 Titicaca (12.08°S, 69.85°W) and Lake Guiers (16.3°N, 16.5°W) (Marchant and
732 Hooghiemstra, 2004).

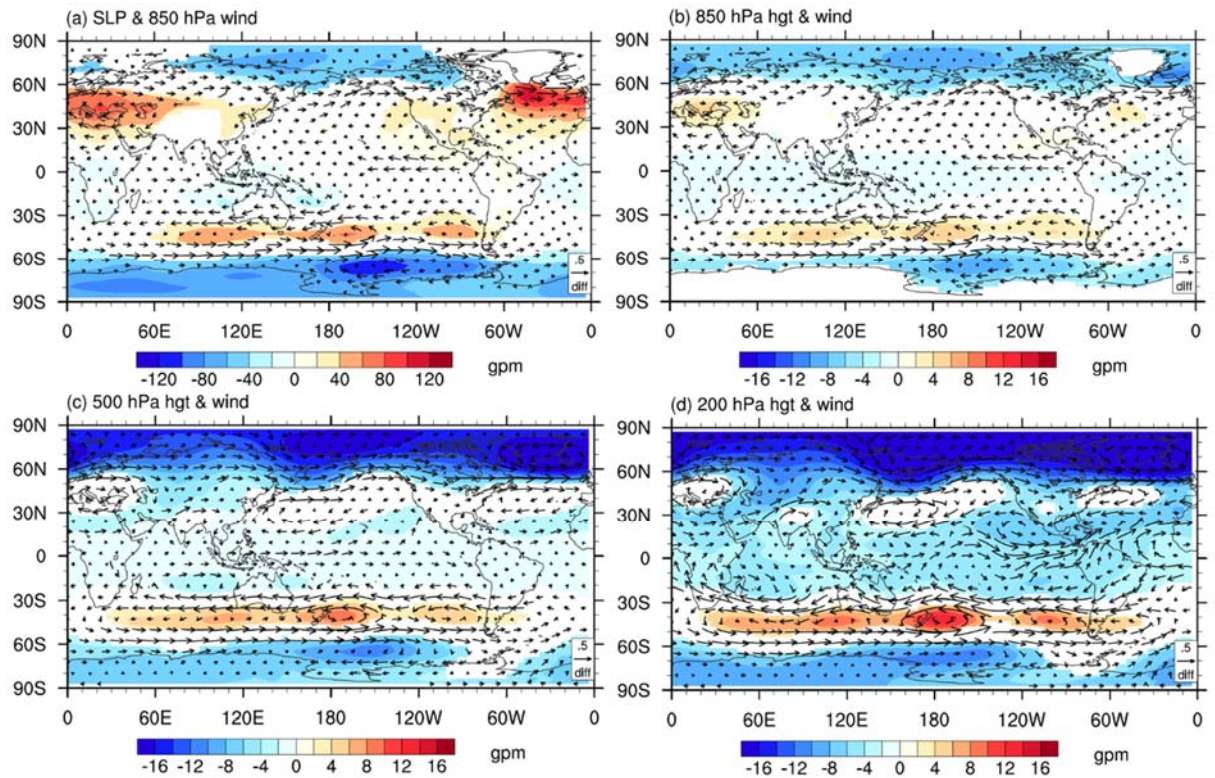
733
734
735
736
737



738
739 **Figure 4** Spatial distribution of annual mean SST difference between the cold and
740 warm periods derived from the TraCE-ALL run. Those regions where significant
741 above 95% confidence level are dotted.
742
743

744

745



746

747 **Figure 5** Differences of annual mean (a) sea level pressure and 850 hPa wind, (b)
748 geopotential height and wind on 850 hPa, (c) geopotential height and wind on 500
749 hPa and (d) geopotential height and wind on 200 hPa between cold and warm periods
750 derived from the TraCE-ALL run. Those regions where significant above 95%
751 confidence level are plotted.

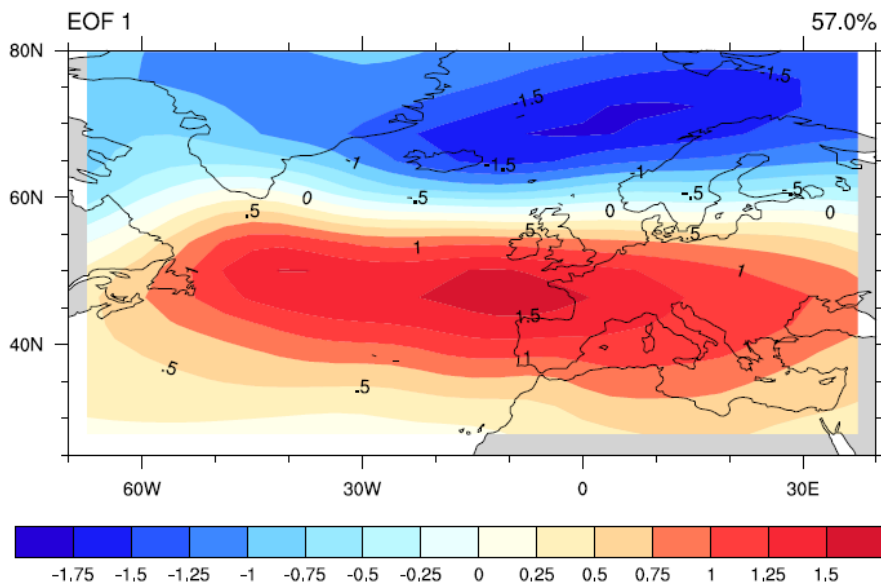
752

753

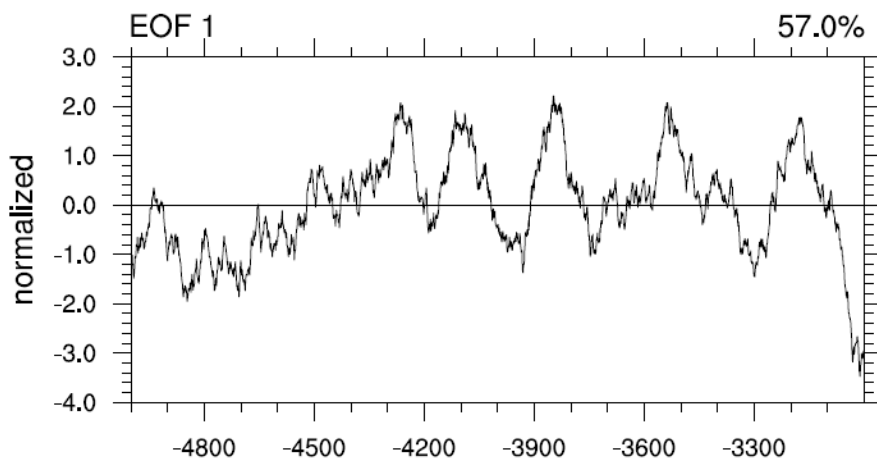
754

755

756



757



758

759 **Figure 6** Standardized first leading mode of the EOF of annual mean SLP over the
760 North Atlantic region (70W-40E, 25N-80N) during the period of 5.0 ka BP to 3.0 ka
761 BP derived from the TraCE-ALL run, after application of a 101-year running mean.
762 The spatial distribution is shown in the top panel, and the time series is shown in the
763 bottom panel. Only this mode passed the North test for EOF.

764

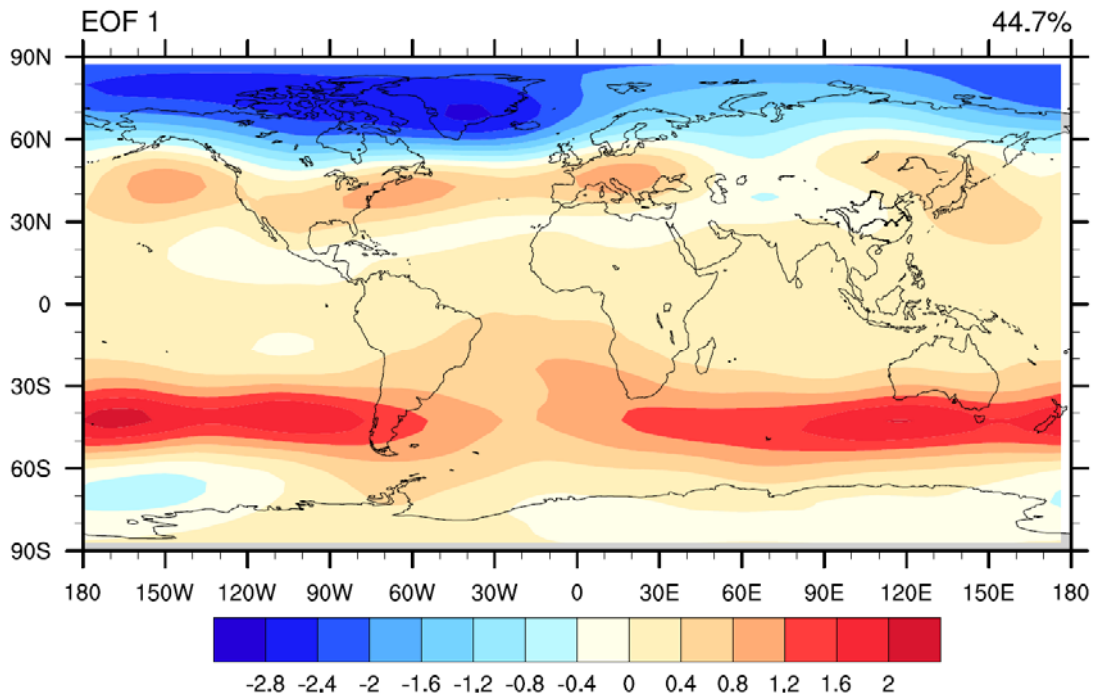
765

766

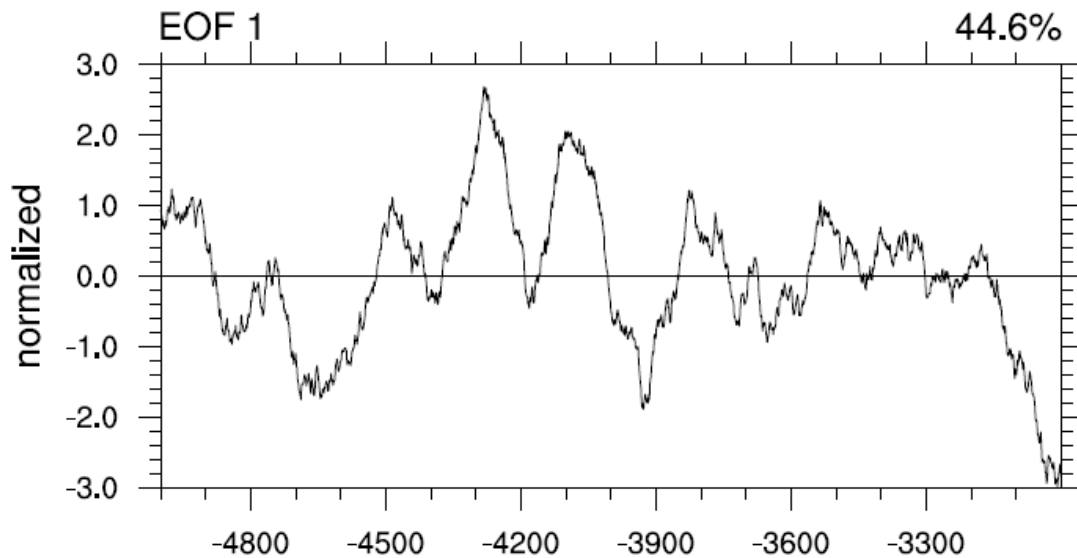
767

768

769
770
771



772

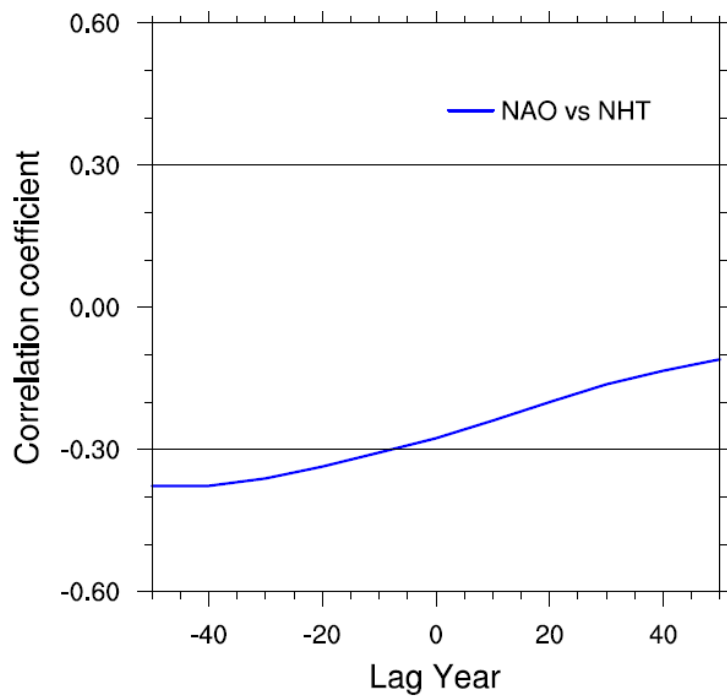


773

774 **Figure 7** Standardized first leading mode of the EOF of annual mean geopotential
775 height at 200 hPa during the period of 5.0 ka BP to 3.0 ka BP derived from the TraCE-
776 ALL run, after application of a 101-year running mean. The spatial distribution is
777 shown in the top panel, and the time series is shown in the bottom panel. Only this
778 mode passed the North test for EOF.

779

780



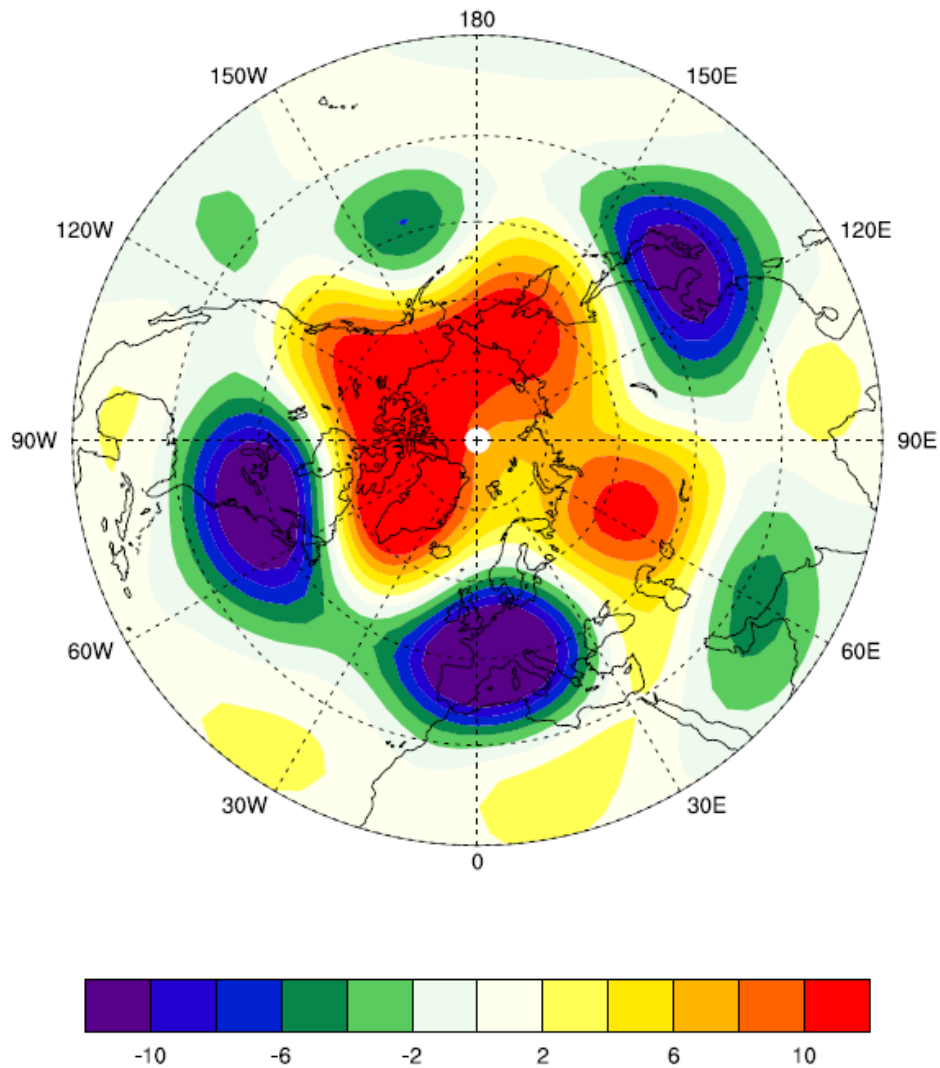
781

782 **Figure 8** Lead-lag correlation between the annual mean North Atlantic Oscillation
783 (NAO) and the North Hemisphere Surface Temperature (NHT) during 4.4 ka BP-4.0
784 ka BP derived from the TraCE-ALL run. The black lines (± 0.3) show the significance
785 levels ($p < 0.05$).

786

787

788



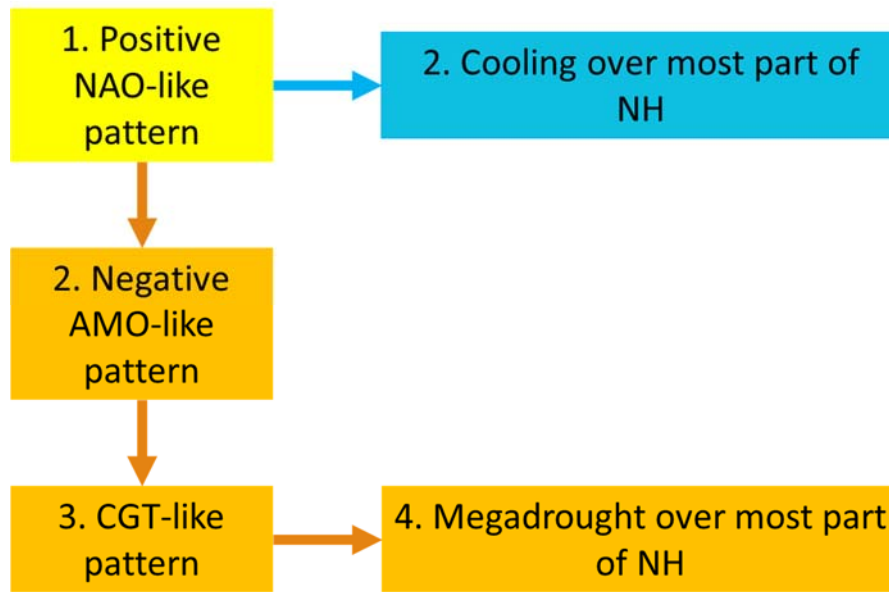
789

790 **Figure 9** Annual mean geopotential height regressed against the SST over the North
 791 Atlantic during 5.0 ka BP - 3.0 ka BP derived from the TraCE-ALL run, after 31-year
 792 running mean application.

793

794

795



796

797 **Figure 10** Schematic diagram shown the mechanisms behind the 4.2 ka BP event.

798

799

800

801 **Table 1** The information of the experiments used in this study.

Experiments	Forcings	Time spanning	Temporal resolution
TraCE-ALL	Orbital, melt-water flux, continental ice-sheet, and Greenhouse gases	22000 BP to 1990 CE	Monthly mean
TraCE-ORB	Orbital only	22000 BP to 1990 CE	Decadal mean
TraCE-MWF	Melt-water flux only	19000 BP to 1990 CE	Decadal mean
TraCE-ICE	Continental ice-sheets only	19000 BP to 1990 CE	Decadal mean
TraCE-GHG	Greenhouse gases only	22000 BP to 1990 CE	Decadal mean

802

803

804

805

806

807

808 **Table 2** Correlation coefficients between the annual mean and seasonal mean NHTs

809 derived from the TraCE-ALL run and those from each single-forcing run from 5.0 ka

810 BP to 3.0 ka BP.

Single forcing run	Annual mean	JJA mean	DJF mean
TraCE-ORB	-0.05	0.79	-0.12
TraCE-MWF	-0.18	0.48	-0.43
TraCE-ICE	-0.30	-0.20	-0.18
TraCE-GHG	0.14	-0.73	0.40

811

812